Proceedings World Geothermal Congress 2026
Calgary, Canada, June 8 – 11, 2026

Mechanisms driving seismicity in hydrothermally active regions

Rahi Abrar[1]*, Mateo Acosta[1*],
1*Department of Geosciences, Virginia Polytechnic Institute and State University, Blacksburg, VA, United States
* Corresponding author: rahi@vt.edu

Keywords: -- Hydrothermal seismicity, hydraulic diffusion, aseismic slip, fault criticality, amplification ratio

ABSTRACT

Seismicity migration in geothermal systems provides valuable insight into subsurface fault dynamics, fluid transport, and stress evolution. It could guide reservoir management decisions for seismic hazard assessment and control. The Salton Sea Geothermal Field (SSGF), located in tectonically active southern California, exhibits recurrent earthquake swarms associated with both natural hydrothermal circulation and anthropogenic operations. Here, we analyze high-resolution earthquake catalogs in the region (Hauksson, Yang, and Shearer, 2012 (HYS)) from 1981–2024 to identify and characterize migrating seismic sequences within the SSGF. Using three-dimensional spatiotemporal migration analysis, we estimate apparent hydraulic diffusivities, characteristic propagation velocities, and characteristic timescales for two earthquake sequences occurring on June 5–9, 2021. The inferred apparent diffusivity values range between 6–150 m^2/s, and migration velocities between 0.3–3.3 km/h, indicating processes significantly faster than those expected from pure pore-pressure diffusion. Applying the analytical framework off Saez et al. (2022), we study how these sequences could be driven by aseismic slip. We derive slip front to fluid front position ratios λ for all sequences. λ is consistently larger than 1 for reasonable values of hydraulic diffusivity at depth demonstrating that the aseismic slip fronts consistently outpace the hydraulic diffusion fronts in the sequences. The main driving mechanism is consistent with fluid-induced aseismic slip (FIAS) rather than direct fluid diffusion (FD). The inferred λ values suggest that the studied faults are critically stressed, where modest fluid injections can drive swarm like migration over kilometer scales in a few hours. Seismicity migration can serve as a diagnostic of fault transmissivity and stress criticality, even in the absence of geodetic data, offering a practical framework for assessing reservoir dynamics and seismic hazard potential in active hydrogeothermal systems.

INTRODUCTION

Geothermal energy is a good alternative to fossil fuels, but developing productive reservoirs is difficult due to their complex fluid dynamics and seismicity potential during stimulation in enhanced geothermal systems or production from conventional hydrothermal systems. In conventional hydrothermal systems, natural fluid circulation through complex fault networks also gives rise to characteristic 'swarm' like migrations (Smith et al., 2009, Roland et al., 2009). These migrations can help determine the hydraulic properties of the subsurface and its state of stress (Debarros et al., 2021). Seismicity migration is commonly explained by fluid pressure diffusion in a medium (FD mechanism; Shapiro et al., 1997, 2002, Rothert and Shapiro 2003). Rising pore pressure lowers the effective normal stress on faults, triggering earthquakes once a failure threshold is reached. The seismic front thus traces the pressure front, both following a diffusive law in time (t): $\boldsymbol{r = \sqrt{4\pi D t}}$ where r is distance and D is the hydraulic diffusivity. This predicts a square-root-of-time growth of seismicity, consistent with many fluid injection driven geothermal observations. More recently, several studies have demonstrated that seismic swarms may be driven by slow, aseismic slip, rather than solely by fluid pressure diffusion (FD mechanism; De Barros et al., 2021, Lohman & McGuire 2007, Sirorattanakul et al. 2022). In such cases, seismicity migrates along with the aseismic slip front (Bhattacharya & Viesca, 2019), which may advance at a rate faster than the fluid pressure front. To describe this behavior, Bhattacharya and Viesca (2019) proposed a model in which the seismic front follows hydraulic diffusion, modified by a scaling factor (λ) such that the inferred apparent diffusivity writes: $D_{app} = \lambda^2 D$. λ accounts for the fault's criticality: how close the initial stress state is to failure. Saez et. al., (2022) developed an analytical solution of dependence of λ on the fault's initial state, the potency of injection, and the hydraulic transmissivity of the fault, potentially allowing to estimate the actual fault's hydraulic diffusivity, and its stress state from seismicity migrations.

The Salton Sea Geothermal Field (SSGF, Figure 1) in the Brawley Seismic Zone, southern California, is a high-heat-flow hydrothermal system that has produced geothermal energy since the 1970s. Persistent seismicity in

the area is linked to fault-guided hydrothermal fluid circulation, with events potentially triggered by either natural or anthropogenic processes. Here, we analyze the seismicity migrations in the SSGF to (1) identify mechanisms behind observed seismic sequences without relying on geodetic data, and (2) constrain fault hydraulic properties at depth, and potentially the stress state.

METHODS

We use the HYS (Hauksson et. al., 2012) which is a manually picked and 3D relocated catalog exhibiting tighter spatial clustering of seismicity than conventional ones. 3D distance of each event was calculated from a reference point at the surface to get the spatial migration of seismicity by projecting the events on a user defined along strike line and then calculating the absolute distance of the projected point from the start of the line as shown in Figure 2B. These reveal multiple migration sequences occurring concurrently. The faults in the region study are highly dipping (>80^o) strike slip presenting significant depth migrations. Thus, we calculated 3-D distances to study the full dynamics. It is noteworthy that due to the 3D relocation of the HYS catalog, the relative depth uncertainty in this catalog should be significantly smaller than in regular catalogs with absolute locations. We fit $\boldsymbol{r = \sqrt{4\pi Dt}}$ curves with an error margin to migrations in shallow and deeper zones to estimate the diffusivity ranges of seismicity migration and linear best fits were used to estimate the migration velocities.

RESULTS

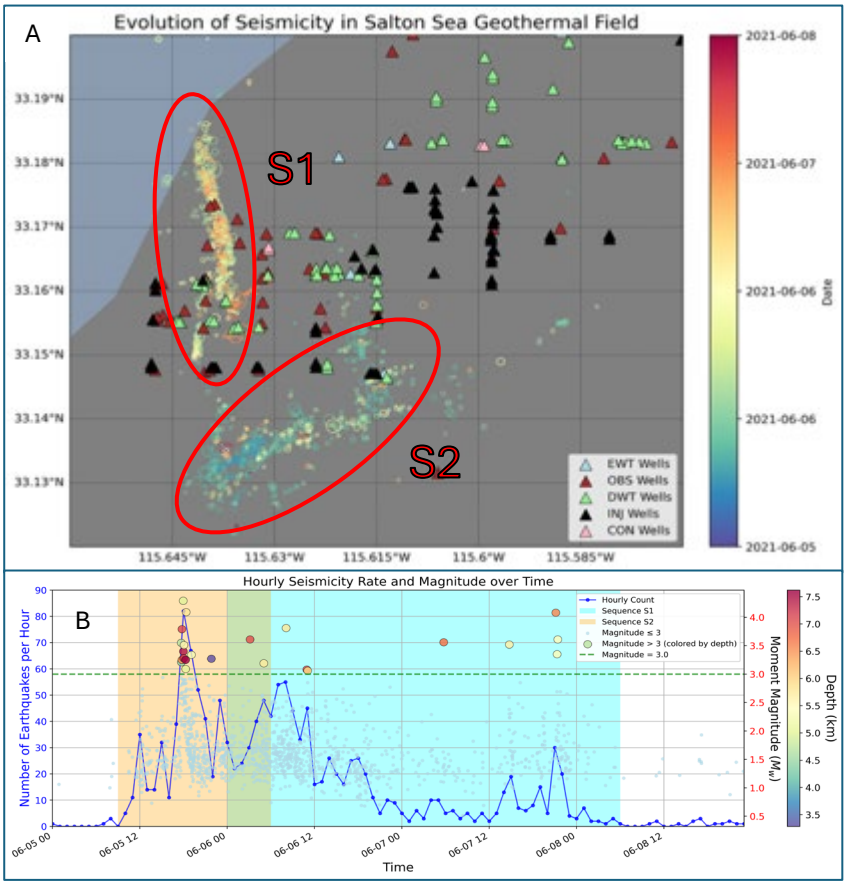


Figure 1: (A) Temporal distribution of seismic events in the Salton Sea Geothermal Field from June 5 to June 8, 2021, superimposed on geothermal well infrastructure. Event locations are color-coded by occurrence date, while triangle symbols denote different well types. Ellipses show the two distinct sequences in space identified in this study. (B) Hourly seismicity rate evolution and magnitude (blue dots) against time. Events above magnitude 3 are color coded by depth. Shaded areas show the temporal evolution of the two studied swarms.

We analyzed the rapid spike in seismic activity in 2021 ranging between dates June 5 to June 8 (Figure 1). We can identify two distinct sequences (Figure 1A): sequences S1 (Figure 2A,B) and S2 (Figure 2C-F). S1 occurs in a fault with strike along NNW-SSE direction and is divided into two temporally distinct sub-sequences S1.1 occurring first, and S1.2 occurring later (Figure 2A). Sequence S2 occurs in a complex U-shaped fault with the main strand in the EW direction and two sub-strands along the NNE-SSW direction (Figure 2B). For S2, we define spatially

distinct sub-sequences S2.1, S2.2, S2.3 (Figure 2C-F). While a slight temporal overlap (S2 dies off between 06-06-00 and 06-06-05 when S1 starts, Figure 1B) in the seismicity rate between the two sequences exists (Figure 1B), a clear spatial separation distinguishes the two sequences (Figure 2C).

SPATIO-TEMPORAL DYNAMICS OF MIGRATION

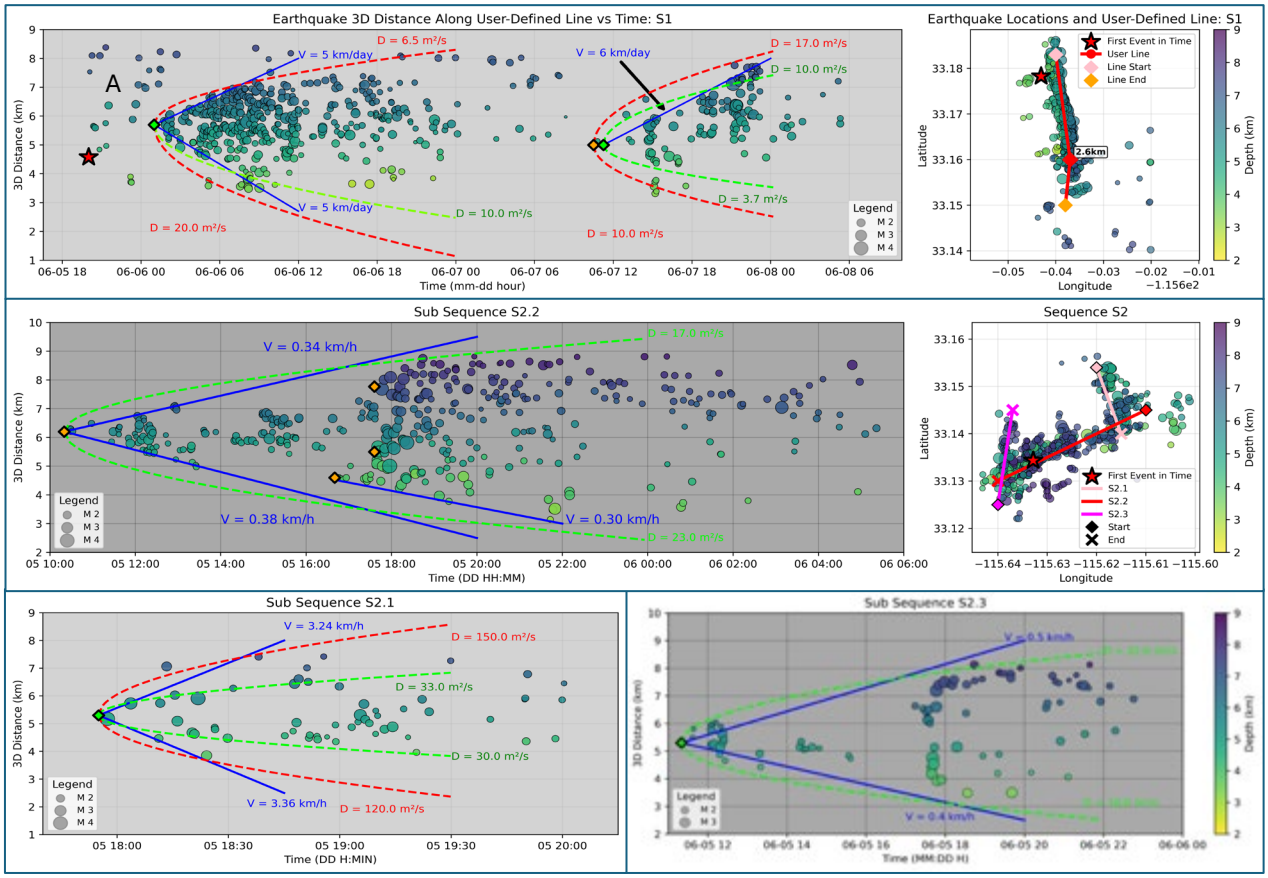


Figure 2: 3-D Space-time evolution of earthquake distances projected from a main fault surface (as defined in panels B and D). Panels A, C, E, F: 3D distance vs time evolution of seismicity for sub sequences S1, S2.1, S2.2, S2.3 respectively. Red and green dashed curves denote square root migration fits to the outer envelopes of seismicity using different ranges of apparent diffusivity values (D), while blue curves are linear fits indicating estimated migration velocities (V). Diamonds show the sub-sequence's initial event(s). Panels B and D: Spatial distribution of the sequences S1 and S2 and defined sub-sequences for S2 (panel D), events are color-coded by depth. Stars represent the first event in time. Colored lines are the defined surface lines for 3D migration calculation with diamonds marking the line start and end.

For sequence S1 (Figure 2A,B) , we identified two sub sequences in time. The first one (S1.1) starts at a depth of 5.7 km from time '06-06 00' and lasts until '06-07 00' and the second one (S1.2) starts at 5 km at time '06-07 12' and lasts till '06-08 00'. Depth limitation is 7 km potentially due to the Brittle-Ductile transition in the region (Violay et al., 2017; Sirorattanakul et al., 2022) and ~2.5 km at shallow depths, where stress accumulation is not sufficient to nucleate earthquakes (Das and Scholz, 1983). For S1.1, the apparent diffusivity for deep to shallow migration ranges between 10-20 m^2/s while the migration toward depth shows D_{app} ~ 6.5 m^2/s. Linear fits indicate velocities of 5 km/day to 7 km/day for deeper and shallower migrations respectively. S1.2 shows D_{app} ~3.7 to 10 m^2/s towards shallow depths and 10 to 17 m^2/s towards higher depths. Velocity is estimated to be 6 km/day towards depth. Shallower migration velocity remains too poorly constrained for this subsequence.

For sequence S2, and its subsequences, Figure 2E shows S2.1 a short lived, fast sequence showing D_{app} 30-120 m^2/s towards shallow depth to 33-150 m^2/s for the migration toward depth. Velocities are 3.36 to 3.24 km/hr respectively. Migration starts at 5 km depth and is constrained within 4-7 km. Subsequence S2.2 (Figure 2C) represented by the pink line in Figure 2D exhibits a characteristic shallow-depth D_{app} in range 23-17 m^2/s and velocities 0.38 to 0.35 km/h. The origin event is at 6 km depth with depth limitations being 2.5 to 8.2 km in shallow and deeper regions respectively. Finally, subsequence S2.3 shows D_{app} ~ 16 to 22 m^2/s for shallower to deeper migrations, and velocities in range 0.4 to 0.5 km/h. Depth limitation is noticeable at 3-8 km with the origin event

at 5.2 km depth. After the subsequence onset, there is no spatial migration until the burst at '06-05 17:30:00' consistent with a jump in seismicity rate (Figure 1B).

DISCUSSION

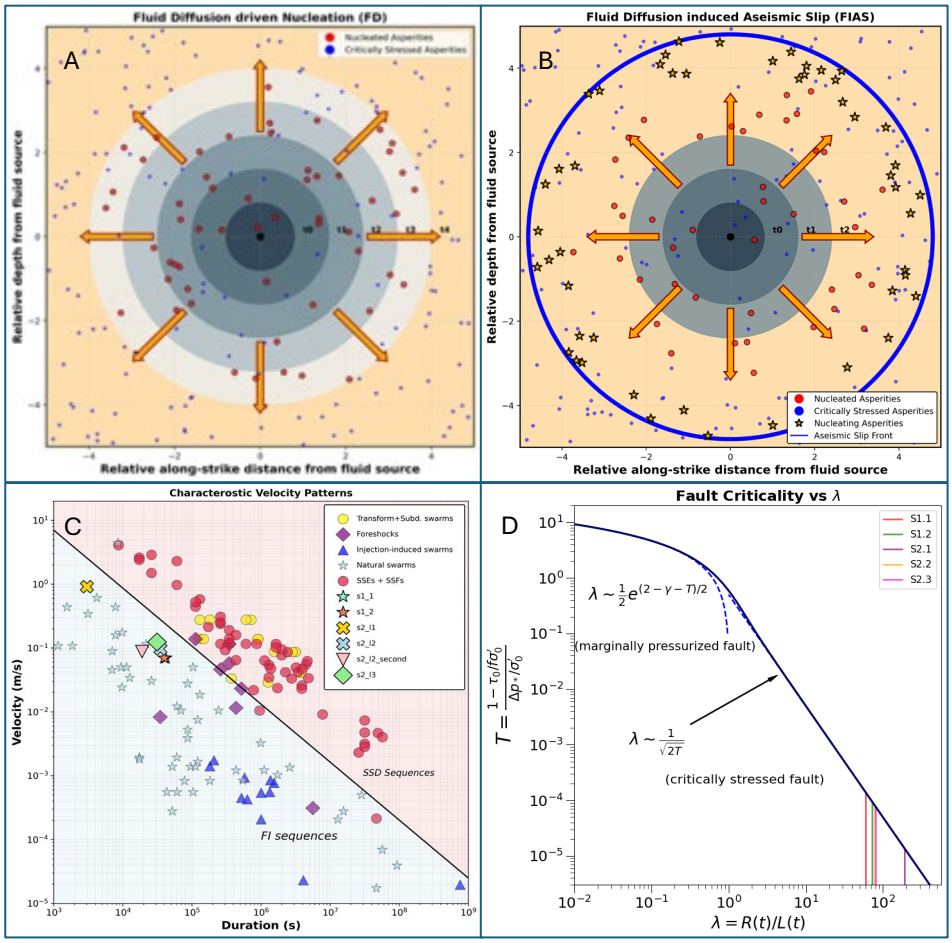


Figure 3: Potential driving mechanisms for SSGF earthquake sequences. A) Fluid diffusion (FD) as the main driving mechanism. Grey contours represent the advancement of a fluid diffusion front which triggers seismic events at potential sources (blue and red critically stressed and nucleated asperities respectively). (B) Fluid induced aseismic slip (FIAS) is the main driving mechanism. Aseismic slip front is the blue line ahead of the diffusion front. Stars represent the seismicity occurring at current time and red dots are nucleated asperities (C) Framework of Danré et al. (2024) distinguishing fluid-induced (FI containing FD and FIAS type mechanisms) and slow-slip–driven (SSD, from natural slow slip events) seismicity globally. Our studied sequences fall well in the upper velocity range of FI sequences. (D) Analytical relation between amplification factor λ and stress-injection parameter for circular ruptures under constant volume-rate injection (modified from Saez et al., 2022). The calculated λ for our swarms is shown as colored lines in the bottom-right section of the plot.

We now try to discriminate between the main driving mechanisms (FD or FIAS, Figure 3A,B) of these sequences from the catalog alone, without need for geodetic data. Seismicity can result from the rupture of critically stressed asperities brought to failure by transient increases in pore pressure from fluid diffusion (Mechanism 1: FD, Figure 3A; Rothert & Shapiro, 2003). Injection lowers the effective normal stress and reactivates these asperities depending on local stress and frictional heterogeneity. As shown in Figure 3A, a central injection source (black point) drives a radially expanding pressure front that sequentially activates nearby asperities (blue) and nucleates slip (red) over time (t_0–t_4) in Figure 3A. On the other hand, seismicity can result from aseismic slip which can transfer stress and drive the critically stressed asperities to failure. This aseismic slip can result from natural tectonic loading (Perfettini et. al., 2010) or from fluid induced aseismic slip (FIAS, Figure 3B).

Danré et al. (2024) proposed an empirical relation of the migration velocity and main driving mechanisms (Figure 3C), where Fluid Induced sequences (FI containing the FIAS and FD mechanisms) distinctively separate in scaling from natural SSE driven seismicity. Placing our inferred characteristic velocities in the Danré relationship

(Figure 3C) shows that our studied (S1.1, S1.2, S2.1, S2.2, S2.3) fall within the FI domain, consistent with one of the fluid-induced mechanisms.

We now analyze whether FD or FIAS are the main driving mechanisms of the SSGF sequences in 2021. Given the observation that most of our sequences show an approximate $\sqrt{t}$ evolution in space, the FIAS front ($R(t)$) migration evolves in a diffusive manner but can be ahead of the fluid pressure front ($L(t) = \sqrt{4\pi. D. t}$). The ratio λ = R(t)/L(t) defines two different regimes: $\lambda < 1$ → FD front is ahead of the FIAS front and $\lambda > 1$ →the FIAS is ahead of the FD. Both fronts begin diffusively, but highly stressed faults later show aseismic slip beyond the pressurized zone (De Barros et al., 2021, Saez et al., 2022). Constraining λ from apparent diffusivities can discriminate between FD and FIAS as the main mechanism driving the sequences. We used estimated of crustal diffusivities to be in the range of 10^{-2} to 10^{-3} m^2/s (Amezawa et. al., (2019)). Using the relation $\lambda = \sqrt{D_{app}/D}$ our calculated λ values to are more than 1, confirming that these sequences are mainly driven by Fluid Induced Aseismic Slip (FIAS).

Saez et al. (2022)'s analysis allows using seismicity migration to potentially constrain fault stress state, fluid transport capacity, and injection parameters. λ is related to a stress-injection parameter $T = (1 - \tau_o/f\sigma_o')/(\Delta p_*/\sigma_o')$ which combines fault stress state and injection strength. Here τ_o is the fault's shear strength, f is friction coefficient and σ_o' is effective normal stress. Using Darcy flow, the injection overpressure is $\Delta p_* = Q_w\eta/4\pi k w_h$ where Q_w is the volumetric flow rate, η is the dynamic viscosity and kw_h the hydraulic transmissivity where k and w_h are permeability and hydraulic aperture respectively. Rearranging the expression for T, we obtain $T = (4\pi k w_h/Q_w\eta)(\sigma_o' - \tau_o/f)$. As λ is inversely proportional to T in the critically stressed regime (Figure 3D, Saez et al., 2022), λ is proportional to the fault's transmissivity (kw_h) and to the stress criticality ($(\sigma_o' - \tau_o/f)$) but inversely proportional to the injection flow rate. Then we can potentially calculate fault's transmissivity from the inferred λ and thus T.

CONCLUSION

By performing high-resolution spatiotemporal analysis of earthquake sequences in the Salton Sea Geothermal Field, we derived apparent diffusivities, migration velocities, and quantified amplification factors of the aseismic slip front to the fluid diffusion front (λ) for individual sequences. All analyzed sequences had characteristic velocities consistent with fluid induced events and apparent diffusivities indicated λ >> 1, so that that aseismic slip systematically outpaces hydraulic diffusion, thus identifying FIAS mechanisms even in the absence of geodetic constraints. This study demonstrates that it is possible to robustly distinguish fluid-induced aseismic slip (FIAS) from direct fluid diffusion (FD) mechanisms in geothermal seismicity using only earthquake catalogs and analytical frameworks, without relying on geodetic or deformation data. Moreover, the diffusivity of seismic sequences could constrain fault transmissivity, an essential parameter for evaluating reservoir connectivity and guiding geothermal development decisions. We thus show how seismicity migration can be used as a robust signal in characterizing reservoir stress states, fault networks and fluid flow.

REFERENCES

Amezawa, Y., Maeda, T. & Kosuga, M. Migration diffusivity as a controlling factor in the duration of earthquake swarms. Earth Planets Space 73, 148 (2021). https://doi.org/10.1186/s40623-021-01480-7

Bhattacharya, P. and Viesca, R. C. (2019) 'Fluid-induced aseismic fault slip outpaces pore-fluid migration', Science, 364(6439), pp. 464–468. doi: 10.1126/science.aaw7354.

Danré, P., Garagash, D., de Barros, L. and Cappa, F. (2024) 'Control of seismicity migration in earthquake swarms by injected fluid volume and aseismic crack propagation', Journal of Geophysical Research: Solid Earth. doi: 10.1029/2023JB027276.

Das, S. and Scholz, C. H. (1983) 'Off-fault aftershock clusters caused by fault zone plasticity', Journal of Geophysical Research: Solid Earth, 88(B6), pp. 4671–4681. doi: 10.1029/JB088iB06p04671.

De Barros, L., Wynants-Morel, N., Cappa, F. and Danré, P. (2021) 'Migration of fluid-induced seismicity reveals the seismogenic state of faults', Journal of Geophysical Research: Solid Earth, 126, e2021JB022767. doi: 10.1029/2021JB022767.

Hauksson, E., Yang, W. and Shearer, P. M. (2012) 'Waveform relocated earthquake catalog for southern California (1981 to June 2011)', Bulletin of the Seismological Society of America, 102(4), pp. 2239–2244. doi: 10.1785/0120120010

Lohman, R. B. and McGuire, J. J. (2007) 'Earthquake swarms driven by aseismic creep in the Salton Trough, California', Journal of Geophysical Research, 112, B04405. doi: 10.1029/2006JB004596.

Park, Y., Mousavi, S. M., Zhu, W., Ellsworth, W. L. and Beroza, G. C. (2020) 'Machine-learning-based analysis of the Guy–Greenbrier, Arkansas earthquakes: A tale of two sequences', Geophysical Research Letters, 47, e2020GL087032. doi: 10.1029/2020GL087032.

Perfettini, H., Avouac, J.-P., Tavera, H., Kositsky, A., Nocquet, J.-M., Bondoux, F., Chlieh, M., Sladen, A., Audin, L., Farber, D. L. and Soler, P. (2010) 'Seismic and aseismic slip on the Central Peru megathrust', Nature, 465, pp. 78–81. doi: 10.1038/nature09062

Roland, E., & McGuire, J. J. (2009). Earthquake swarms on transform faults. Geophysical Journal International, 178(3), 1677-1690.

Rothert, E. and Shapiro, S. A. (2003) 'Microseismic monitoring of borehole fluid injections: Data modeling and inversion for hydraulic properties of rocks', GEOPHYSICS, 68, pp. 685–689. doi: 10.1190/1.1567239.

Ross, Z. E., Cochran, E. S., Trugman, D. T. and Smith, J. D. (2020) '3D fault architecture controls the dynamism of earthquake swarms', Science, 368(6497), pp. 1357–1361. doi: 10.1126/science.abb0779.

Sáez, A., Lecampion, B., Bhattacharya, P. and Viesca, R. C. (2022) 'Three-dimensional fluid-driven stable frictional ruptures', Journal of the Mechanics and Physics of Solids, 160, 104754. doi: 10.1016/j.jmps.2021.104754.

Shapiro, S. A., Huenges, E., Borm, G. (1997) 'Estimating the crust permeability from fluid-injection-induced seismic emission at the KTB site', Geophysical Journal International, 131(2), pp. F15–F18. doi: 10.1111/j.1365-246X.1997.tb01215.x.

Shapiro, S. A., Rothert, E., Rath, V. and Rindschwentner, J. (2002) 'Characterization of fluid transport properties of reservoirs using induced microseismicity', Geophysics, 67(1), pp. 212–220.

Sirorattanakul, K., Ross, Z. E., Khoshmanesh, M., Cochran, E. S., Acosta, M. and Avouac, J.-P. (2022) 'The 2020 Westmorland, California earthquake swarm as aftershocks of a slow slip event sustained by fluid flow', Journal of Geophysical Research: Solid Earth, 127(11), e2022JB024693. doi: 10.1029/2022JB024693.

Smith, R., Jordan, M., Steinberger, B., Puskas, C., Farrell, J., Waite, G. P., Husen, S., Chang, W. and O'Connell, R. (2009) 'Geodynamics of the Yellowstone hotspot and mantle plume: Seismic and GPS imaging, kinematics, and mantle flow', Journal of Volcanology and Geothermal Research, 188(1–3), pp. 26–56. doi: 10.1016/j.jvolgeores.2009.08.020.

Violay, M., Heap, M. J., Acosta, M. and Madonna, C. (2017) 'Porosity evolution at the brittle-ductile transition in the continental crust: Implications for deep hydro-geothermal circulation', Scientific Reports, 7(1), 7705. doi: 10.1038/s41598-017-08108-5.